# In-Depth Studies on Rapid Photochemical Activation of Various Sol–Gel Metal Oxide Films for Flexible Transparent Electronics

*Sungjun Park, Kwang-Ho Kim, Jeong-Wan Jo, Sujin Sung, Kyung-Tae Kim, Won-June Lee, Jaekyun Kim, Hyun Jae Kim, Gi-Ra Yi, Yong-Hoon Kim, Myung-Han Yoon,* and Sung Kyu Park**

**Despite intensive research on photochemical activation of sol–gel metal oxide materials, the relatively long processing time and lack of deep understanding of the underlying chemical courses have limited their broader impact on diverse materials and applications such as thin-film electronics, photovoltaics, and catalysts. Here, in-depth studies on the rapid photochemical activation of diverse sol–gel oxide films using various spectroscopic and electrical investigations for the underlying physicochemical mechanism are reported. Based on the exhaustive chemical and physical analysis, it is noted that deep ultraviolet-promoted rapid film formation such as densification, polycondensation, and impurity decomposition is possible within 5 min via in situ radical-mediated reactions. Finally, the rapid fabrication of all-solution metal oxide thin-film-transistor circuitry, which exhibits stable and reliable electrical performance with a mobility of >12 $cm^2 V^{-1} s^{-1}$ and an oscillation frequency of >650 kHz in 7-stage ring oscillator even after bending at a radius of <1 mm is demonstrated.**

## 1. Introduction

The increasing demand for large-area, flexible, low-cost electronics for nonconventional displays,[1] wearable[2,3] and ultralight[4] devices, and disposable circuits[5,6] requires development of high-performance electronic materials and economical fabrication processes. Metal oxide materials have emerged as a promising platform[7–9] as these materials demonstrated great potential for transparent electrodes,[10–14] high-mobility semiconductors,[15–26] and high-k dielectrics.[27–31] Based on sol–gel chemistry, it is of particular interest because solid metal oxide materials with excellent electrical characteristics can be easily synthesized from small molecular precursors via simple solution processes, which herald a new era of very large-area electronics at an affordable cost. To convert an integrated network of colloidal sol–gel particles to highly pure, fully densified metal oxide films, the following steps should be completed: i) energy must be supplied to facilitate metal–oxygen–metal (M—O—M) bond formation (*polycondensation*); ii) solubilizing metal ligands (e.g., alkoxide, nitrate, chloride), condensation by-products (e.g., water, alcohol), solvents, and stabilizer molecules must be removed through evaporation/decomposition (*impurity removal*); iii) the interconnected gel film with substantial voids must be compactly densified (*film densification*). In this regard, such an as-deposited coarse film inevitably requires high-temperature activation step due to low thermal conductivity.

Recently, many researchers have attempted to develop low-temperature annealing processes for solution-deposited metal-oxide semiconductors, particularly for utilization on flexible plastic substrates. These approaches include judicious

S. Park, S. Sung, W.-J. Lee, Prof. M.-H. Yoon
School of Materials Science and Engineering
and Research Institute for Solar and Sustainable Energies
Gwangju Institute of Science and Technology
Gwangju 500-712, South Korea
E-mail: mhyoon@gist.ac.kr

K.-H. Kim, J.-W. Jo, K.-T. Kim, J. Kim, Prof. S. K. Park
Devices and
Displays Research Laboratory
Chung-Ang University
Seoul 156-756, South Korea
E-mail: skpark@cau.ac.kr

K.-H. Kim, J.-W. Jo, K.-T. Kim, J. Kim, Prof. S. K. Park
School of Electrical and Electronics Engineering
Chung-Ang University
Seoul 156-756, South Korea

K.-H. Kim, Prof. H. J. Kim
School of Electrical and Electronics Engineering
Yonsei University
Seoul 120-749, South Korea

Prof. G.-R. Yi
School of Chemical Engineering
Sungkyunkwan University
Suwon 440-746, South Korea

Prof. Y.-H. Kim
School of Advanced Materials Science and Engineering
Sungkyunkwan University
Suwon 440-746, South Korea

**DOI: 10.1002/adfm.201500545**

precursor formulations using labile metal ligands,[17] non-carbon solvents,[14,18,19] dopants[20,30] or combustion fuel additives[21] as well as noble postdeposition treatments relying on ozone exposure,[22] laser/microwave annealing,[23,24] and ultraviolet activation.[25,26,31,32] However, despite the growing utility in large-area flexible electronics, only a few studies have been reported on reducing process temperature and time together for sol–gel derived dielectric materials (Table S1 and Figure S1) (Supporting Information), because oxide dielectrics typically require prolonged thermal annealing time at considerable higher temperature than semiconductors to guarantee pinhole-free and densified films for minimal leakage current with high capacitance values. Such time-consuming requirements in process condition typically deter prompt preparation of sol–gel metal oxide dielectric films and scalable fabrication of all-solution-processed, high-performance metal oxide transistor arrays on unconventional substrates.

Most importantly, to fully realize all-solution-processed metal oxide flexible circuitry, it is highly desirable to establish a generalized methodology for rapid conversion of as-deposited xerogel-like oxide materials to high-quality thin-films at low temperatures while effectively removing metal ligands, condensation by-products, and other chemical impurities during M—O—M network formation,[33] using a various types of general metal oxide precursors. For this purpose, deep ultraviolet (DUV) irradiation was employed because high-energy photons are assumed to optically penetrate into various oxide materials, homogeneously induce photoinitiated radical-forming reactions, and energetically activate the chemical bonds[25,26,31,34,35] involved in the abovementioned chemical processes only with moderate heating (**Figure 1**). In this work, we report the rapid photochemical activation generalized to various sol–gel MOx dielectrics and in-depth chemical and physical analyses to unveil underlying physicochemical mechanism based on photo-induced radical-mediated reactions. We further demonstrate that general sol–gel derived metal oxide dielectric films can be rapidly densified in 5 min, and all-solution-processed flexible metal oxide transistor arrays could be successfully fabricated on both glass and ultra-flexible plastic substrates.

## 2. Results and Discussion

A low-pressure mercury lamp (LPML, 253.7 and 184.9 nm) was chosen as a low-power economical DUV source due to its minimal unintentional heating, large-area coverage, and mass-production scalability, unlike conventional high-power excimer laser systems, which relies predominantly on photothermal annealing.[23] All sol–gel metal oxide films were spin-coated onto $n^+$–Si substrates using corresponding metal precursor solutions, and photochemically activated in an oxygen-free environment such that direct DUV absorption and in situ photochemical reactions would not be hindered by ozone formation. Subsequently, a variety of film characterizations were performed and compared in between the sol–gel metal oxide films with and without DUV irradiation at various posttreatment times. As demonstrated by the ellipsometric film analysis (**Figure 2**a), DUV exposure induces dramatic reduction in film thickness, leading to the fast (<5 min) formation of dense aluminum oxide layers. In the case of no DUV exposure, the resultant film thickness gradually decreased with increasing annealing time; however, the measured value after 1 h (13 nm) was still higher than that for the photoactivated film after 5 min (10 nm). Furthermore, as shown in the inset of Figure 2a, other types of sol–gel dielectrics ($ZrO_x$ (i), $ZrO_x$ (ii), $HfO_x$) also exhibit the same type of rapid densification under DUV irradiation, suggesting the generality of DUV-based photoactivation at low temperatures and widening the selection of oxide-based gate dielectric materials available for plastic substrates (vide infra). In Figure 2b, the attenuated total reflectance Fourier transform infrared (ATR-FT-IR) spectra reveal that the intensities of the broad IR absorption bands centered at ≈3500 $cm^{-1}$ (O—H stretching) and ≈1650 $cm^{-1}$ (H—O—H bending)[36,37] in photoactivated sol–gel films for 5 min rapidly decreased to the levels of those annealed at high temperature (350 °C). The other prominent feature in the FT-IR spectra of photoannealed films is the disappearance of the absorption bands centered at 1400 and 1340 $cm^{-1}$, which are ascribed to the N—O stretching modes in nitrate ligand.[38] These results distinctly indicate that DUV photochemical activation effectively accelerates the reduction of surface O—H functional group density and the removal of water molecules and nitrate ligands within 5 min, and that the extent of photoactivation effect is equivalent to that observed in films that have been thermally annealed at 350 °C for 1 h.

Regarding the aforementioned DUV effect, we hypothesized that the incident high-energy photons immediately generate radicals via photolysis of residual (metal) ligands inside porous film and that rapid radical-mediated reactions assist prompt formation of high-quality metal oxide films and decomposition of chemical impurities into small gaseous molecules. For instance, the in situ generation of $NO_2$ and OH radicals via nitrate photocleavage upon DUV absorption[39,40] is described below (Equation (1)) in the case that metal nitrate salt is used as a sol–gel precursor.

$$NO_3^- \rightarrow \cdot NO_2 + \cdot OH \quad (1)$$

In Figure 2c, the UV–vis spectra of a photoactivated aluminum nitrate solution clearly show the growing vibronic bands of nitrous acid (HONO),[41] a protonated form of $NO_2$ radical[39,40] as a product of photodecomposition. In addition, the proton nuclear magnetic resonance (H-NMR) spectrum of a mixture of aluminum nitrate and benzene under DUV conditions exhibits the in situ formation of OH radicals as confirmed by the proton peaks originated from phenol, the product due to the reaction between benzene and photogenerated OH radical (Figures 2d and S2, Supporting Information).[39,42] $NO_2$ and OH radicals are known to be highly reactive to hydrogen capture followed by subsequent M—OH activation for efficient M—O—M polycondensation and other complex radical-mediated reactions with undesired residual chemical species. Indeed, gas chromatography–mass spectrometry (GC–MS) results obtained under DUV-exposure conditions exhibit many peaks attributed to small molecular by-products from various radical-mediated reactions in solution and as-spun film, thereby supporting the abovementioned photo-induced radical hypothesis (Figures 2e and S3–5, Supporting Information). These

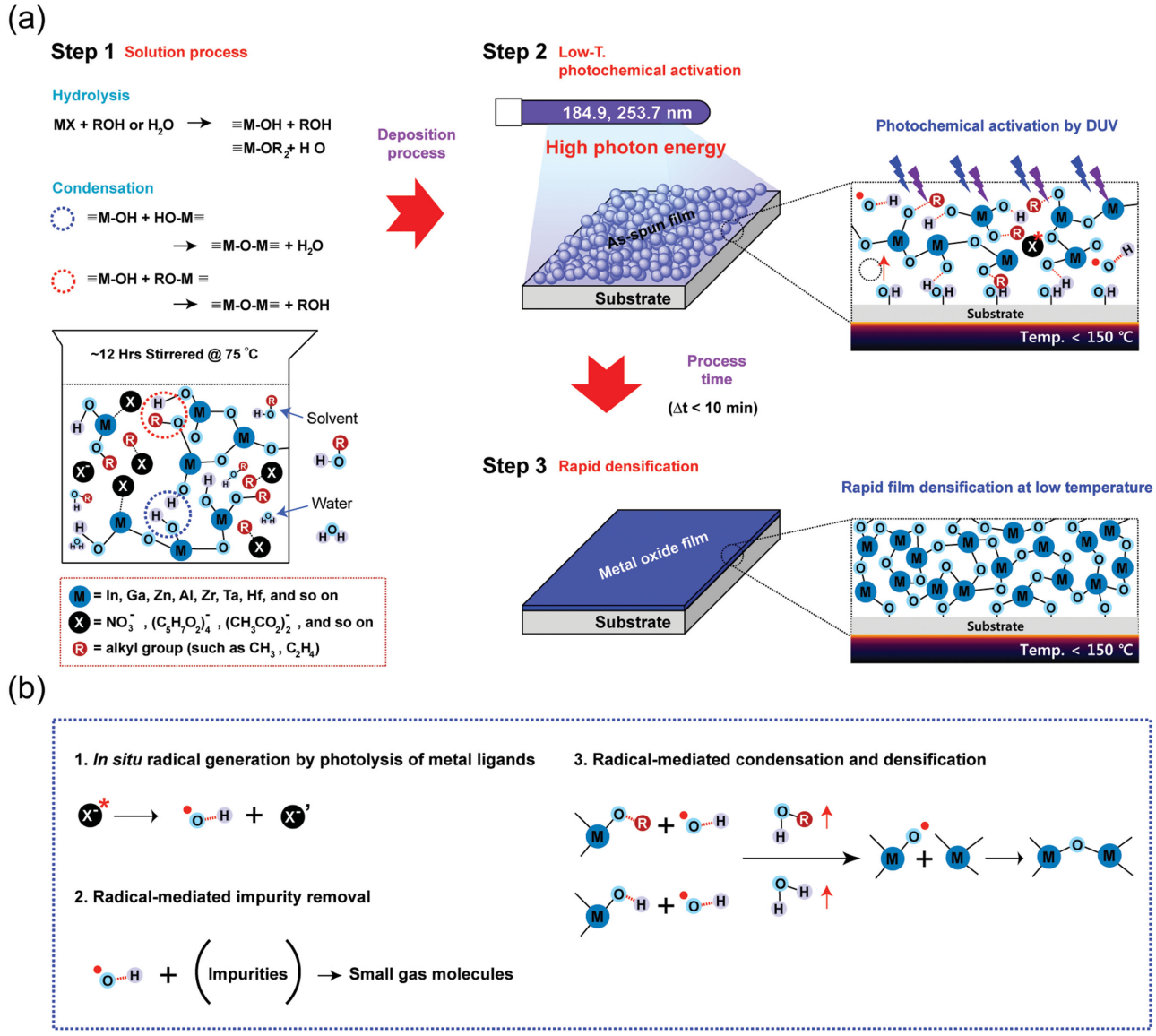


**Figure 1.** Photoactivation of sol–gel metal oxide materials and the proposed mechanism. a) Overall schematic illustration of the rapid low-temperature photoactivation of various sol–gel metal oxide films. b) Proposed physicochemical mechanism of the rapid low-temperature photoactivation process via photochemical activation (direct photodecomposition of impurities, in situ radical formation, enhancement of rapid condensation and densification).

photo-induced reactive radicals are supposed to be uniformly generated from photocleavable ligands and consequent radical-assisted *local* processes are highly effective in promoting M—O bond formation and film densification throughout the entire solid film compared with the conventional thermal activation (see also Figure S6, Supporting Information).

In addition to rapid film densification, the degrees of polycondensation and impurity removal are also of critical importance, particularly for insulator purpose. The chemical states of the O(1*s*), N(1*s*), and C(1*s*) electrons were closely examined via x-ray photoelectron spectroscopy (XPS). **Figure 3**a presents a series of deconvoluted O(1*s*) XPS spectra of sol–gel aluminum oxide films annealed under different annealing conditions. Interestingly, the photochemical activated oxide film exhibited an XPS profile similar to that of the high-temperature-annealed film, featuring a dominant contribution at 531.0 eV (Al—O—Al) and a minimal signature of Al—O—H at 532.3 eV.[43,44] By contrast, the thermally activated film exhibited a gradual shift with increasing temperature, from the profile of the as-spun film to that of the film annealed at 350 °C (Table S2 and Figures S7–S9, Supporting Information). These results indicate that the polycondensation reaction is promoted upon DUV irradiation, and the resultant photoactivated film exhibited a considerably lower M—OH density at the same substrate temperature. The residual amounts of nitrogen and carbon elements inside the films were also monitored. The disappearance of the N(1*s*) and C(1*s*) peaks in the XPS spectra[30,45–48] of the photochemically activated films reveals that DUV irradiation effectively decomposes the nitrate ligands and solvent molecules residing in the as-spun film into diffusible small-molecular species due

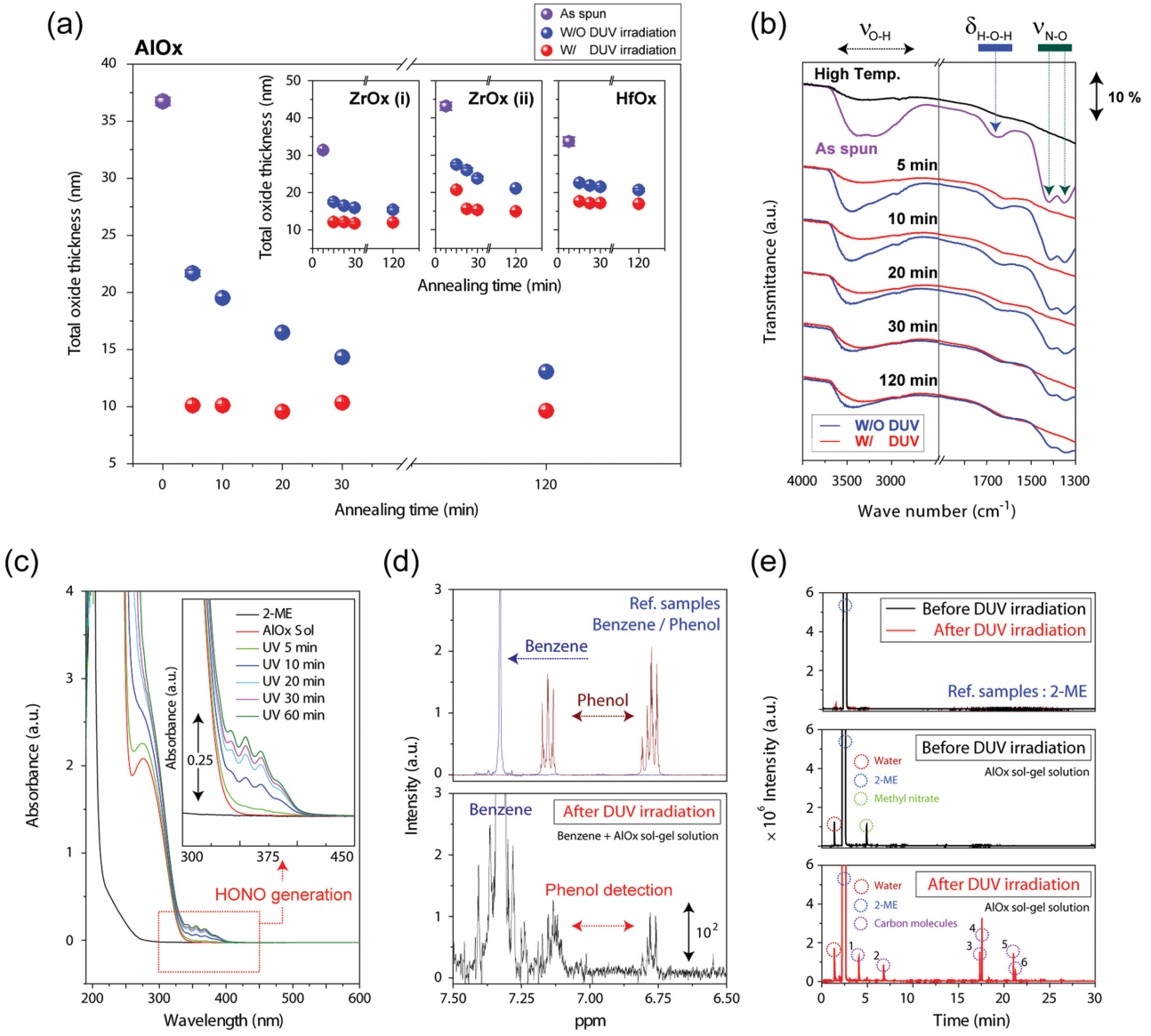


**Figure 2.** Effects of rapid photoactivation on the sol–gel metal oxide films. a) Thickness analysis of aluminum oxide films thermally annealed at 150 °C as a function of annealing time without (blue dots) and with (red dots) DUV irradiation (data averaged over five experiments). The insets show the results for various sol–gel-derived metal oxide films composed of different ligands under the same experimental conditions (ZrOx (i): from zirconium nitrate, ZrOx (ii): from zirconium acetylacetonate, HfOx: from hafnium isopropoxide). b) ATR-FT-IR spectra of aluminum oxide films maintained at 150 °C without (blue line) and with (red line) DUV irradiation as a function of exposure time. c) UV–vis spectra of a 2-methoxyethanol (2-ME) solvent (black line) and aluminum oxide sol–gel solutions as a function of DUV irradiation time. The inset presents a magnified plot of the data showing the growth of the vibronic bands of HONO with increasing DUV irradiation time. d) 400 MHz $^1$H NMR spectra of benzene and phenol as references (top) and of aluminum oxide sol–gel precursors and benzene in $CD_3OD$ after 4 h of DUV irradiation (bottom). The appearance of the phenol proton peak indicates the formation of OH radicals under DUV irradiation (see the main text for details). e) Gas chromatograms (GCs) of the 2-ME solvent immediately before (black line) and after 1 h of DUV irradiation (red line) as a reference (top) and of the aluminum oxide sol–gel solution before (center panel) and after 1 h of DUV irradiation (bottom).

to direct photodecomposition or radical-induced reactions (Figure 3b,c). Furthermore, the time-of-flight secondary ion mass spectrometry (TOF-SIMS) 3D mapping of residual elements indicates that carbon contamination was dramatically reduced throughout the entire film depth of the photoactivated oxide materials, whereas a substantial amount of carbon was still confined inside thermally annealed films (Figures 3d and S10,S11, Supporting Information). Therefore, such a low level of residual impurities in photoannealed films is one of the convincing explanation for low leakage currents observed in photochemically activated sol–gel dielectric films (vide infra).

The temperature effect on photochemical activation was further interrogated to understand how modest heating interplays with the aforementioned photochemical activation for exceptionally fast formation of highly dense, highly pure metal oxide films. Ellipsometric analysis of the overall oxide film thickness

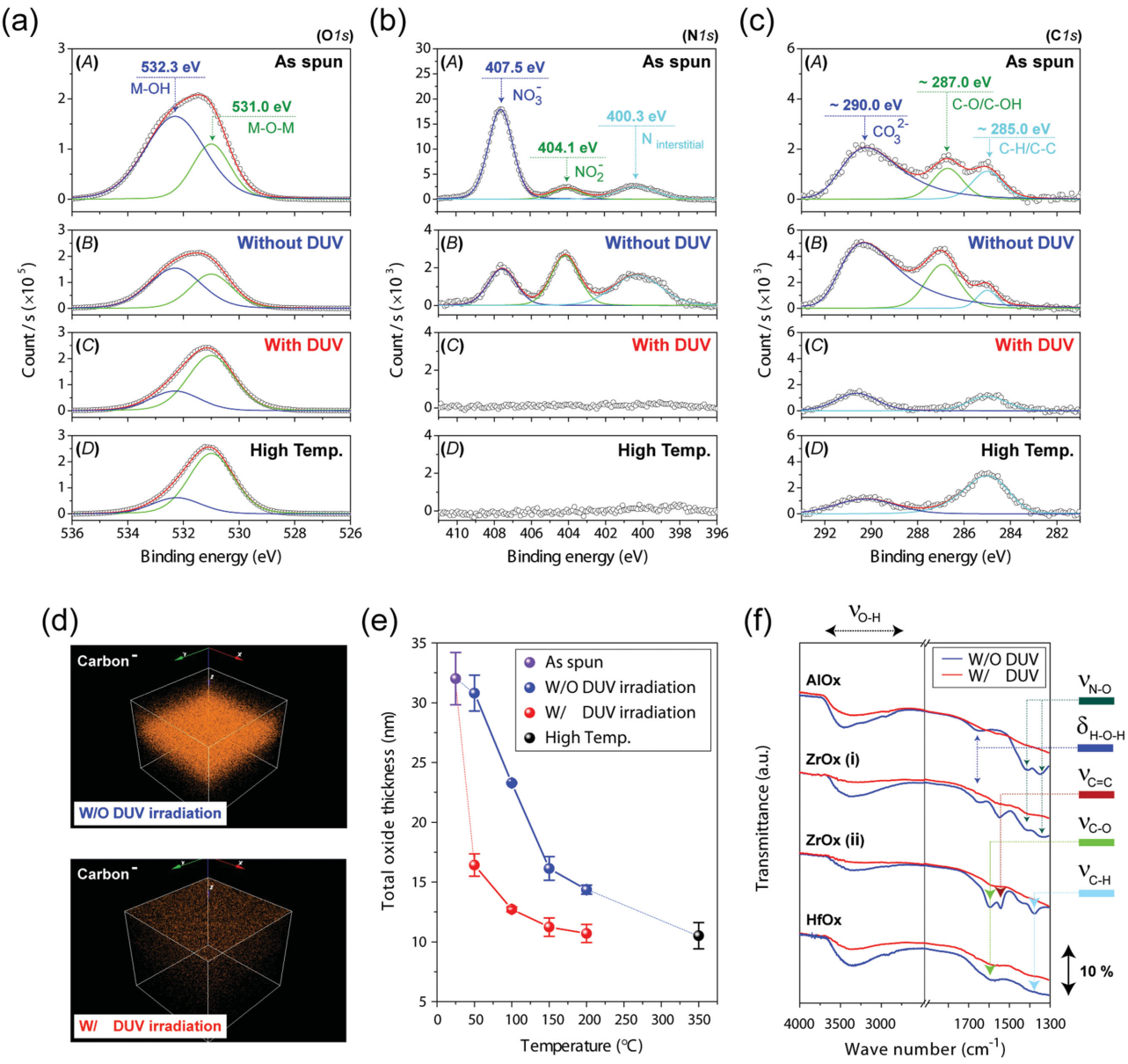


**Figure 3.** Temperature effect on the DUV photoactivation of sol–gel metal oxide films. Deconvoluted XPS spectra of aluminum oxide films in the spectral regions of a) O(1s), b) N(1s), and c) C(1s): from top to bottom, each panel displays the spectra of A) the as-spun film, a film that was maintained at 100 °C for 5 min B) without and C) with DUV irradiation, and D) a film that was thermally annealed at 350 °C for 60 min. d) TOF-SIMS 3D mapping images of negative carbon ions inside aluminum oxide films maintained at 150 °C without (top) and with (bottom) DUV irradiation. e) Variation in the thicknesses of sol–gel aluminum oxide films maintained at 150 °C without and with DUV irradiation (each data point averaged over five experiments). f) ATR-FT-IR spectra of various thin metal oxide films maintained at 100 °C without (blue line) and with (red line) DUV irradiation for 5 min (ZrOx (i): from zirconium nitrate, ZrOx (ii): from zirconium acetylacetonate, HfOx: from hafnium isopropoxide).

reveals that the short DUV exposure substantially reduced the final oxide film thickness from 33 nm (as spun) to 16 nm at 50 °C and to 11 nm at 150 °C (Figure 3e). The additional effect of gentle heating during DUV annealing was marginal once substrate temperature was raised above 150 °C. We suppose that photogenerated radicals chemically activated the M—O bonds and induced the tight packing of the initially coarse M—O—M networks. During DUV treatment, moderate heating induced both the accelerated diffusion of decomposed small molecular impurities and the thermal agitation (i.e., vibration) for lowering the activation barrier for M—O bond-forming condensation, leading to very fast film densification compared with DUV photoactivation without gentle heating. The atomic force microscopy result also indicates that DUV irradiation at 150 °C assisted in smoothing the initially rough oxide surface, presumably through the aforementioned mechanism (Figures S12,S13, Supporting Information). Previously, effective densification of rough oxide films was achieved only by using very intense, high-energy light sources, for instance, excimer lasers[23] or synchrotron radiation.[34,35]

In parallel, the generality of photochemical activation method was examined using various types of metal ligand precursor solutions ($AlO_x$, $ZrO_x$ (i), $ZrO_x$ (ii), $HfO_x$). As shown in the ATR-FT-IR spectra (Figure 3f), all of the photoactivated oxide dielectric films exhibit significantly higher transmittance in spectral regions corresponding to OH stretching and ligand-specific vibration modes,[36–38] implying that rapid photochemical activation can be achieved using various photocleavable ligands (i.e., nitrate, acetylacetonate, isopropoxide). Unlike the related articles focusing on a single oxide dielectric material, mostly $ZrO_x$,[26,30,31] our photochemical process appears to be applicable to various types of both dielectric and semiconducting films, as confirmed by electrical characterization presented below. To our knowledge, this is the first report that solid scientific evidence has been provided on the generalization of low-temperature photochemical activation to various sol–gel metal oxide materials and the proposition of radical-mediated photochemical mechanisms on rapid (<5 min) densification and impurity removal.

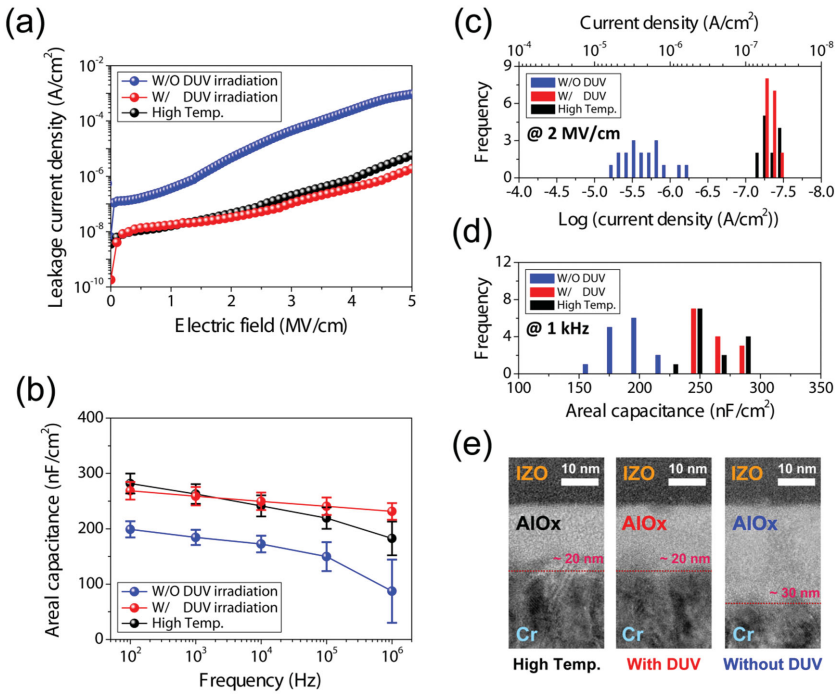


**Figure 4.** Electrical characteristics and TEM images of sol–gel metal oxide dielectrics. a) Leakage current density–electric field (*J–E*) plot and b) capacitance–frequency (*C–F*) plot for sol–gel aluminum oxide films maintained at 150 °C for 30 min without (blue) and with DUV irradiation (red) and thermally annealed at 350 °C for 60 min (black). All dielectric film devices (≈20 nm) were prepared from 0.3 M precursor solutions in the configuration of metal(IZO)-insulator-metal(Cr) (MIM). Also presented are the statistical distributions of c) the leakage current densities at 2 MV/cm and d) the areal capacitances at 1 kHz as well as e) cross-sectional transmission electron micrographs of the sol–gel aluminum-oxide-based MIM devices.

To confirm that the integrity of the photochemically activated dielectric and semiconducting films translated into their electrical performance, metal–insulator–metal (MIM) and thin-film transistor (TFT) devices based on DUV-annealed sol–gel oxide dielectrics were fully characterized. For electrical device fabrication, thicker film deposition (≈20 nm) and a longer photoactivation time (30 min) were employed to ensure the conformal coverage of the metal oxide films on the patterned metal (Cr) electrodes and minimal variation in device characteristics, although less than 5 min of DUV exposure was sufficient for photoactivation of thinner oxide films on unpatterned electrodes. **Figure 4**a,b present the leakage current density–electric field (*J–E*) and capacitance–frequency (*C–F*) plots of the sol–gel-derived aluminum oxide films on metal-patterned glass substrates. In contrast to the thermally annealed films, the photochemically activated films exhibit sufficiently low leakage current densities (2–6 × $10^{-8}$ A $cm^{-2}$ at 2 MV $cm^{-1}$) with a high breakdown field (≈8 MV $cm^{-1}$) and high capacitance (250–300 nF $cm^{-2}$ at 1 kHz) with low frequency dependence. A statistical analysis of the measured leakage current density and areal capacitance of the photoactivated devices exhibit substantially lower leakage current densities, stronger breakdown fields, and higher areal capacitances than those annealed without DUV irradiation (Figures 4c,d and S14, Supporting Information). These performance metrics, which are comparable with or slightly better than those of the sol–gel dielectric films annealed at 350 °C, were achieved only with single-layered photoactivated films without any protective layers on top, such as additional metal oxide[26–28,30] or self-assembled molecular layers.[31] Similarly, photoactivated sol–gel zirconium and hafnium oxide films exhibit excellent dielectric performance (Figure S15, Supporting Information). Such dielectric properties are consistent with the result in cross-sectional transmission electron microscopy (TEM) images showing very dense film of photoactivated aluminum oxide in MIM device (Figure 4e). These results well match the aforementioned observation that the in situ photochemical reactions assisted the high-quality sol–gel film formation through rapid film densification (Figure 2) and efficient impurity elimination (Figure 3) at relatively low temperatures (<150 °C). This unprecedentedly fast photochemical process may be a breakthrough in the transition to the large-scale fabrication of functional metal–oxide-based device arrays on ultraflexible plastic substrates using various recipes for solution-processed oxide materials and an economical flood-exposure DUV light source based on a low-power mercury lamp.

Large-area sol–gel metal oxide TFT circuitry was fabricated using two consecutive photoannealing processes for both gate dielectric and semiconducting layers on the same substrate. To evaluate the present process for its broad compatibility with various substrates and feasibility for large-area mass production, borosilicate glass (≈0.5-mm thick) and spin-on-polyimide (PI, ≈3-μm thick) were employed; these are the most widely-used substrate materials in the research of large-area displays and ultraflexible electronics, respectively. The transfer and output characteristics of the $InO_x$ TFTs on the glass substrates are presented in **Figure 5**a,b, respectively, revealing that the average field-effect mobility was 8.33 $cm^2$ $V^{-1}$ $s^{-1}$ with a

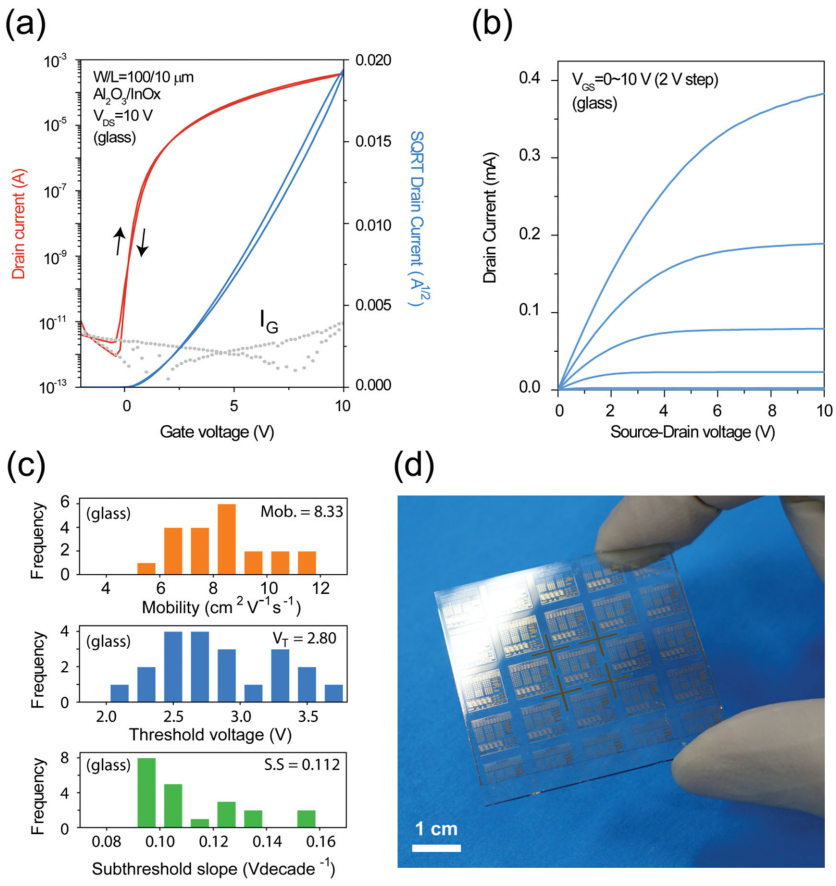


**Figure 5.** All-solution-processed and entirely photoactivated metal-oxide devices and circuitry on glass substrates. a) Double-sweep transfer curves and b) corresponding output characteristics of photoactivated $AlO_x/InO_x$ TFTs on glass. c) Statistical distributions of field-effect mobilities, threshold voltages, and subthreshold slopes of photoactivated $AlO_x/InO_x$ TFTs on glass. d) Photographs of transparent devices and circuits based on $AlO_x/InO_x$ TFTs constructed on glass substrates.

narrow distribution (Figure 5c). These results are comparable with those for TFT devices fabricated directly on silicon substrates (Figures S16,S17, Supporting Information). Note that the remarkable electrical performance with high mobility and negligible hysteresis of the $InO_x/AlO_x$ TFTs demonstrates that excellent interfacial properties as well as high-quality sol–gel oxide film structure can be obtained via rapid photoactivation despite its low processing temperature (<150 °C).

Furthermore, to address the scientific and industrial implications of photochemically activated sol–gel metal–oxide materials for the development of ultraflexible electronics, the TFT arrays, which included 7-stage ring oscillator circuitry constructed on the ultrathin PI films, were released from the underlying buffer glass substrate and characterized under more practical conditions. To minimize the creation of surface defects and the subjection of the material to undesired mechanical stress during the release process, a thin polymer layer (≈400 nm) was overcoated on top of the final device arrays. As shown in **Figure 6**a, the released photochemically activated gate dielectrics and semiconductors exhibited no cracks or defects, even under severe bending conditions. The measured electrical characteristics of the $InO_x/AlO_x$ TFTs and circuits on the ultrathin PI substrates are presented in Figure 6b–d, illustrating that the average field-effect mobility was 8.02 $cm^2$ $V^{-1}$ $s^{-1}$ with a threshold voltage of 3.67 V; this performance is comparable with that of TFT devices fabricated directly on glass substrates (Figure S18, Supporting Information). Despite repetitive bending and release, the electrical properties of the TFT devices and integrated circuits remained uncompromised with respect to those of the as-fabricated devices. The resultant ultraflexible ring oscillator circuitry exhibited extremely stable and reliable electric properties, demonstrating a mobility of >10 $cm^2$ $V^{-1}$ $s^{-1}$ and an oscillation frequency of >650 kHz (at a supply bias of 15 V) even after bending at the smallest radius tested (R < 1 mm). This result attests that the rapid photoactivation process enabled the conversion of the solution-processed oxide-based materials into highly stable and reliable gate dielectrics and semiconductors directly on ultra-flexible plastic substrates and that the electrical performance of the consequent circuitry was sufficiently tolerant to mechanical stress.

## 3. Conclusions

In this article, we report on a generalized photochemical activation route for preparing high-quality sol–gel metal oxide dielectrics as well as semiconductors, and the rapid fabrication of all-solution-processed transistor arrays. A comprehensive investigation based on spectroscopic and surface analyses was pursued to unveil the underlying physicochemical mechanism based on in situ radical formation and moderate heating through which DUV-based photochemical activation is dramatically effective in terms of the subsequent film densification, polycondensation promotion, and impurity removal. The present thermally-assisted photochemical activation route will serve as a general methodology to enable the preparation of all solution large-area flexible displays and ultraflexible wearable electronics in a rapid, scalable, and economic manner.

## 4. Experimental Section

*Preparation of Sol–Gel Precursor Solutions*: Each prepared precursor solution (0.1–0.3 M of aluminum nitrate nonahydrate, zirconium acetylacetonate, zirconium oxynitrate hydrate, or hafnium isopropoxide isopropanol adduct was dissolved in 5 mL of 2-ME solvent and then vigorously stirred for more than 12 h at 75 °C; all reagents for synthesis were purchased from Sigma-Aldrich) was filtered through a 0.2 μm PTFE syringe filter and spin coated onto the substrate.

*Optical and Surface Characterization*: UV–vis absorption spectra were obtained using a Lambda 750 UV–vis/NIR spectrophotometer (Perkin-Elmer). GC–MS (GC-6890N; MS-5973; Agilent Technologies) was used for the chemical analysis of the gas samples and precursor solutions. The

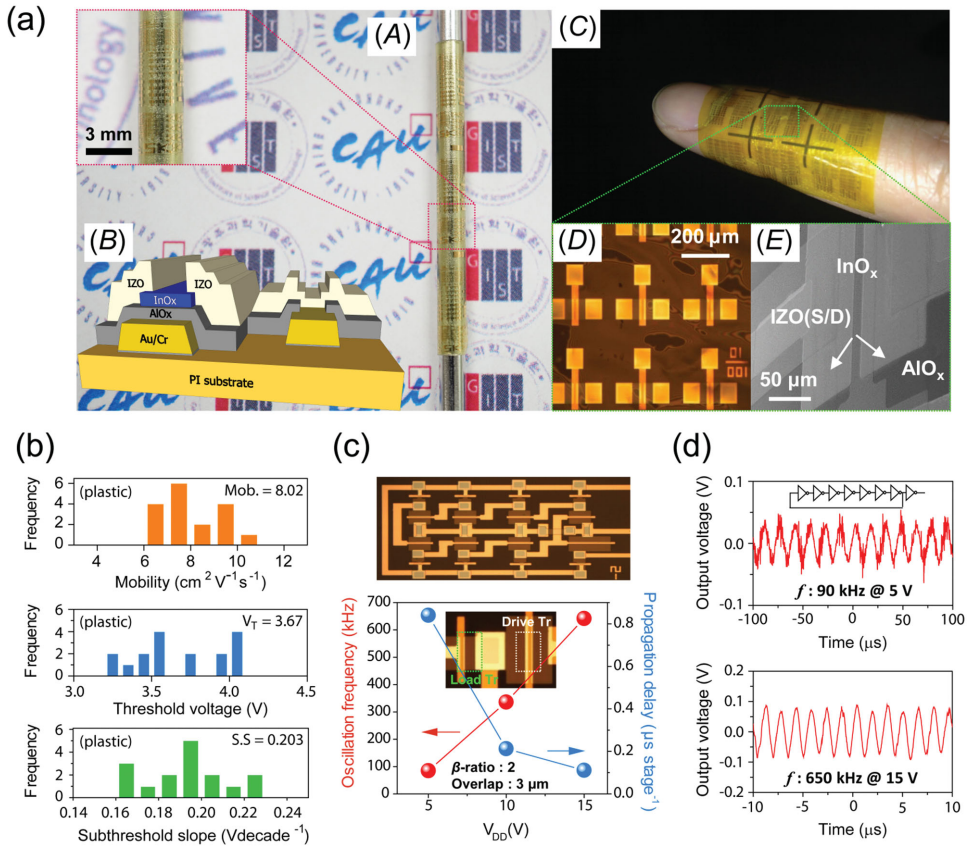


**Figure 6.** All-solution-processed and entirely photoactivated metal-oxide devices and circuitry on ultraflexible PI substrates. a) Photographs of ultrathin and patchable $AlO_x/InO_x$ TFT-based circuits constructed on ultrathin plastic substrates (≈3 μm): The resultant circuits transferred to rolled over A) a spatula (r = 1.5 mm) and B) a human finger; C) the 3D device schematics (photoactivated AlOx/InOx TFTs); and D) an optical micrograph of TFTs on PI film. E) Scanning electron microscope (SEM) image of crack-free device on curved PI. b) Statistical distributions of the measured field-effect mobilities, threshold voltages, and subthreshold slopes of the photoactivated $AlO_x/InO_x$ TFTs on PI substrates. c) Oscillation frequency (red) and per-stage propagation delay (blue) of a 7-stage ring oscillator as a function of the supply voltage, $V_{DD}$. d) Output waveforms of the 7-stage ring oscillator operating with supply voltages of 5 V (top panel) and 15 V (bottom panel) and at oscillation frequencies of 90 and 650 kHz.

FT-IR spectra of the oxide films deposited on $n^+$-Si wafers were obtained using a 660-IR (Varian) with a grazing-angle ATR accessory (Seagull, Harrick) in nitrogen-purging condition. The XPS spectra were obtained using K-alpha (Thermo VG) after argon sputter cleaning was performed to minimize the unintentional carbon contamination. The TOF-SIMS data were obtained using a TOF-SIMS V instrument (ION-TOF GmbH).

*Device Fabrication and Measurement*: Photochemically activated metal-oxide films were fabricated using a high-density ultraviolet treatment system with a low-pressure Hg lamp (emission wavelengths of 253.7 (90%) and 184.9 nm (10%); area of 20 × 20 $cm^2$; DUV253H, Filgen) under $N_2$-purging conditions. For the fabrication of solution-processed dielectrics on a heavily doped $n^+$–Si substrate or a patterned Cr electrode, the samples were photoannealed in an $N_2$ atmosphere for 30 min after the spin-coating process. Then, an Au (overlapped area of 300 × 300 $μm^2$) or IZO (overlapped area of 110 × 130 $μm^2$) top electrode, respectively, was deposited on the dielectric layer. For the fabrication of solution-processed metal-oxide TFTs on glass and polymeric substrates, glass substrates of 0.5 mm in thickness (Eagle 2000TM, Samsung Corning Precision Glass) and spin-on-polyimide substrates with patterned gated electrodes were used. The dielectric and semiconducting layers were continuously photoannealed in an $N_2$ atmosphere for 30 min after the spin-coating process. IZO source/drain electrodes (100 nm in thickness) were deposited using the conventional lift-off technique. After the completion of metal oxide devices on ultrathin flexible film, the fully-fabricated devices were over-coated by ≈400-nm-thick PMMA layer to protect the surface and to minimize the applied stress imposed on the devices during the detaching process. Then, flexible devices were released from a carrier glass substrate. The detached flexible film rolls up instantly (bending radius less than 1 mm) and was immersed into a water to flatten the rolled films. Floated PI film can be transferred onto flat glasses to measure the electrical characteristics.

## Supporting Information

Supporting Information is available from the Wiley Online Library or from the author.

## Acknowledgements

S.P., K.-H.K., and J.-W.J. contributed equally to this paper. The authors thank Dr. J. S. Jin and Miss D. Y. Kim for helpful analyses and discussions with TOF-SIMS at Korea Basic Science Institute (KBSI) Busan center. This research was partially supported by the National Research Foundation of Korea (NRF) grant funded by the Korea government (MSIP) (No. NRF-2013R1A2A2A01006404). Also, this work was supported by the Center for Advanced Soft-Electronics funded by the Ministry of Science, ICT and Future Planning as Global Frontier Project (2011-0031639), South Korea.

Received: February 9, 2015
Revised: March 9, 2015
Published online: March 30, 2015

[1] C. Wang, D. Hwang, Z. Yu, K. Takei, J. Park, T. Chen, B. Ma, A. Javey, *Nat. Mater.* **2013**, *12*, 899.
[2] G. Schwartz, B. C.-K. Tee, J. Mei, A. L. Appleton, D. H. Kim, H. Wang, Z. Bao, *Nat. Commun.* **2013**, *4*, 1859.
[3] D. Son, J. Lee, S. Qiao, R. Ghaffari, J. Kim, J. E. Lee, C. Song, S. J. Kim, D. J. Lee, S. W. Jun, S. Yang, M. Park, J. Shin, K. Do, M. Lee, K. Kang, C. S. Hwang, N. Lu, T. Hyeon, D.-H. Kim, *Nat. Nanotechnol.* **2014**, *9*, 397.
[4] M. Kaltenbrunner, T. Sekitani, J. Reeder, T. Yokota, K. Kuribara, T. Tokuhara, M. Drack, R. Schwödiauer, I. Graz, S. Bauer-Gogonea, S. Bauer, T. Someya, *Nature* **2013**, *499*, 458.
[5] S.-W. Hwang, H. Tao, D.-H. Kim, H. Cheng, J.-K. Song, E. Rill, M. A. Brenckle, B. Panilaitis, S. M. Won, Y.-S. Kim, Y. M. Song, K. J. Yu, A. Ameen, R. Li, Y. Su, M. Yang, D. L. Kaplan, M. R. Zakin, M. J. Slepian, Y. Huang, F. G. Omenetto, J. A. Rogers, *Science* **2012**, *337*, 1640.
[6] S. Bauer, M. Kaltenbrunner, *ACS Nano* **2014**, *8*, 5380.
[7] K. Nomura, H. Ohta, K. Ueda, T. Kamiya, M. Hirano, H. Hosono, *Science* **2003**, *300*, 1269.
[8] J. F. Wager, *Science* **2003**, *300*, 1245.
[9] E. M. C. Fortunato, P. M. C. Barquinha, A. C. M. B. G. Pimentel, A. M. F. Gonçalves, A. J. S. Marques, R. F. P. Martins, L. M. N. Pereira, *Appl. Phys. Lett.* **2004**, *85*, 2541.
[10] R. B. H. Tahar, T. Ban, Y. Ohya, Y. Takahashi, *J. Appl. Phys.* **1998**, *83*, 2631.
[11] B. G. Lewis, D. C. Paine, *MRS Bull.* **2000**, *25*, 22.
[12] T. Minami, *Semicond. Sci. Technol.* **2005**, *20*, S35.
[13] Z. Chen, W. Li, R. Li, Y. Zhang, G. Xu, H. Cheng, *Langmuir* **2013**, *29*, 13836.
[14] H. Hagendorfer, K. Lienau, S. Nishiwaki, C. M. Fella, L. Kranz, A. R. Uhl, D. Jaeger, L. Luo, C. Gretener, S. Buecheler, Y. E. Romanyuk, A. N. Tiwari, *Adv. Mater.* **2014**, *26*, 632.
[15] D.-H. Lee, Y.-J. Chang, G. S. Herman, C.-H. Chang, *Adv. Mater.* **2007**, *19*, 843.
[16] Y.-J. Chang, D.-H. Lee, G. S. Herman, C.-H. Chang, *Electrochem. Solid-State Lett.* **2007**, *10*, H135.
[17] K. K. Banger, Y. Yamashita, K. Mori, R. L. Peterson, T. Leedham, J. Rickard, H. Sirringhaus, *Nat. Mater.* **2011**, *10*, 45.
[18] S. T. Meyers, J. T. Anderson, C. M. Hung, J. Thompson, J. F. Wager, D. A. Keszler, *J. Am. Chem. Soc.* **2008**, *130*, 17603.
[19] Y. Hwan Hwang, J.-S. Seo, J. Moon Yun, H. Park, S. Yang, S.-H. Ko Park, B.-S. Bae, *NPG Asia Mater.* **2013**, *5*, e45.
[20] S. Jeong, Y.-G. Ha, J. Moon, A. Facchetti, T. J. Marks, *Adv. Mater.* **2010**, *22*, 1346.
[21] M.-G. Kim, M. G. Kanatzidis, A. Facchetti, T. J. Marks, *Nat. Mater.* **2011**, *10*, 382.
[22] S.-Y. Han, G. S. Herman, C. Chang, *J. Am. Chem. Soc.* **2011**, *133*, 5166.
[23] Y.-H. Yang, S. S. Yang, K.-S. Chou, *IEEE Electron Device Lett.* **2010**, *31*, 969.
[24] T. Jun, K. Song, Y. Jeong, K. Woo, D. Kim, C. Bae, J. Moon, *J. Mater. Chem.* **2011**, *21*, 1102.
[25] Y.-H. Kim, J.-S. Heo, T.-H. Kim, S. Park, M.-H. Yoon, J. Kim, M. S. Oh, G.-R. Yi, Y.-Y. Noh, S. K. Park, *Nature* **2012**, *489*, 128.
[26] Y.-H. Lin, H. Faber, K. Zhao, Q. Wang, A. Amassian, M. McLachlan, T. D. Anthopoulos, *Adv. Mater.* **2013**, *25*, 4340.
[27] J. T. Anderson, C. L. Munsee, C. M. Hung, T. M. Phung, G. S. Herman, D. C. Johnson, J. F. Wager, D. A. Keszler, *Adv. Funct. Mater.* **2007**, *17*, 2117.
[28] S. T. Meyers, J. T. Anderson, D. Hong, C. M. Hung, J. F. Wager, D. A. Keszler, *Chem. Mater.* **2007**, *19*, 4023.
[29] B. N. Pal, B. M. Dhar, K. C. See, H. E. Katz, *Nat. Mater.* **2009**, *8*, 898.
[30] J. H. Park, Y. B. Yoo, K. H. Lee, W. S. Jang, J. Y. Oh, S. S. Chae, H. W. Lee, S. W. Han, H. K. Baik, *ACS Appl. Mater. Interfaces* **2013**, *5*, 8067.
[31] Y. M. Park, J. Daniel, M. Heeney, A. Salleo, *Adv. Mater.* **2011**, *23*, 971.
[32] J.-W. Jo, J. Kim, K.-T. Kim, J.-G. Kang, M.-G. Kim, K.-H. Kim, H. Ko, Y.-H. Kim, S. K. Park, *Adv. Mater.* **2015**, *27*, 1182
[33] L. L. Hench, J. K. West, *Chem. Rev.* **1990**, *90*, 33.
[34] H. Imai, K. Awazu, M. Yasumori, H. Onuki, H. Hirashima, *J. Sol-Gel Sci. Technol.* **1997**, *8*, 365.
[35] H. Imai, H. Hirashima, K. Awazu, *Thin Solid Films* **1999**, *351*, 91.
[36] G. Socrates, *Infrared and Raman Characteristic Group Frequencies: Tables and Charts*, John Wiley & Sons, New York **2004**.
[37] H. A. Al-Abadleh, V. H. Grassian, *Langmuir* **2003**, *19*, 341.
[38] D. J. Goebbert, E. Garand, T. Wende, R. Bergmann, G. Meijer, K. R. Asmis, D. M. Neumark, *J. Phys. Chem. A* **2009**, *113*, 7584.
[39] J. Mack, J. R. Bolton, *J. Photochem. Photobiol. Chem.* **1999**, *128*, 1.
[40] S. Goldstein, J. Rabani, *J. Am. Chem. Soc.* **2007**, *129*, 10597.
[41] J. Stutz, E. S. Kim, U. Platt, P. Bruno, C. Perrino, A. Febo, *J. Geophys. Res. Atmospheres* **2000**, *105*, 14585.
[42] P. Warneck, C. Wurzinger, *J. Phys. Chem.* **1988**, *92*, 6278.
[43] J. van den Brand, W. G. Sloof, H. Terryn, J. H. W. de Wit, *Surf. Interface Anal.* **2004**, *36*, 81.
[44] P. K. Nayak, M. N. Hedhili, D. Cha, H. N. Alshareef, *Appl. Phys. Lett.* **2013**, *103*, 033518.
[45] J. Baltrusaitis, P. M. Jayaweera, V. H. Grassian, *Phys. Chem. Chem. Phys.* **2009**, *11*, 8295.
[46] I. V. Plyuto, A. P. Shpak, I. V. Babich, Y. V. Plyuto, L. F. Sharanda, J. Stoch, J. A. Moulijn, *Surf. Interface Anal.* **1999**, *27*, 911.
[47] S. Feliu Jr, M. C. Merino, R. Arrabal, A. E. Coy, E. Matykina, *Surf. Interface Anal.* **2009**, *41*, 143.
[48] K. Shimizu, C. Phanopoulos, R. Loenders, M.-L. Abel, J. F. Watts, *Surf. Interface Anal.* **2010**, *42*, 1432.